RSC Advances

PAPER

View Article Online
View Journal | View Issue

Cite this: *RSC Adv.*, 2024, **14**, 16713

Targeting EGFR/PI3K/AKT/mTOR signaling in lung and colon cancers: synthesis, antitumor evaluation of new 1,2,4-oxdiazoles tethered 1,2,3-triazoles†

Mohammed Salah Ayoup, *[ab] Islam Shawki,[b] Hamida Abdel-Hamid,[b] Doaa A. Ghareeb,[cg] Aliaa Masoud,[c] Marwa F. Harras,[d] Mohamed El-Atawy, *[be] Nuha Salamah Alharbi[f] and Magda M. F. Ismail[d]

Received 23rd March 2024
Accepted 12th May 2024

DOI: 10.1039/d4ra02222j

rsc.li/rsc-advances

The EGFR/PI3K/Akt/mTOR pathway is important for metastasis, medication resistance, apoptosis prevention, and malignant transformation. Mutations in lung and colon cancer typically change this pathway's expression. As a result, a novel class of 1,2,4-oxdiazoles that are attached to 1,2,3-triazoles, **5–11**, were created as possible anticancer drugs. The produced compounds are all examined by spectroscopic and micro-analytical techniques. MTT assay results on lung (A549) colon (Caco-2) and normal lung fibroblast (WI38) revealed that compounds **6a**, **6b**, **8a**, and **11b** demonstrated strong and selective antiproliferative activities against lung (A549) and colon (Caco-2) cancer cell lines while the remaining derivatives showed moderate to low activity. qPCR data revealed that the potential hits had large fold changes in the downregulation of EGFR, mTOR, and PI3K; they upregulate the amount of p53 to support their mode of action even more. Interestingly, docking investigations validated the biological outcomes by demonstrating a strong affinity of our compounds against EGFR active regions. Computational predictions of all the synthesized compounds' pharmacokinetic profiles, physicochemical characteristics, and drug-likeness data indicated that the promising hits might be taken into consideration as drug-like prospects.

1. Introduction

Humanity is currently engaged in a struggle with a number of health-related issues, particularly those pertaining to cancer. This has fueled the desire to create strong, targeted inhibitors of tumor cells that would specifically target oncogenic proteins that play critical roles in the development and spread of cancer.[1]

Because of its involvement in oncogenesis, EGFR is one of the receptors that has been investigated the most.[2] Numerous cancer forms, including colorectal cancer,[3] non-small-cell lung cancer (NSCLC),[4] squamous cell carcinoma of the head and neck,[5] glioblastoma,[6] pancreatic cancer,[7] and breast cancer,[8] have been linked to the proto-oncogenic activity of EGFR. Globally, lung cancer is now the primary cause of cancer-related mortality.[9] In advanced non-small cell lung cancer (NSCLC), individuals with EGFR mutations have been first-line treated with epidermal growth factor receptor tyrosine kinase inhibitors (EGFR-TKIs). However, the clinical efficacy of this treatment is significantly limited by drug resistance that develops following continuous and prolonged chemotherapy. To combat medication resistance, it is crucial to develop novel chemotherapeutic agents and treatment approaches. Likewise, EGFR is thought to be overexpressed in 60–80% of tumors in colorectal cancer (CRC), and this is linked to a poor prognosis.[10] These factors have contributed to the targeting of EGFR as a therapeutic target for monoclonal antibodies and small molecule inhibitors, the former of which is used to treat metastatic illness.[11]

EGFR/PI3K/AKT/mTOR signaling is a key pathway in many different kinds of cancer. This route positively controls a number of cellular functions, such as metabolism, migration, survival, and proliferation. Additionally, it is essential in

[a]*Department of Chemistry, College of Science, King Faisal University, Al-Ahsa 31982, Saudi Arabia. E-mail: mayoup@kfu.edu.sa; mohammedsalahayoup@gmail.com*
[b]*Department of Chemistry, Faculty of Science, Alexandria University, Alexandria, Egypt. E-mail: mohamed.elatawi@alexu.edu.eg*
[c]*Bio-screening and Preclinical Trial Lab, Biochemistry Department, Faculty of Science, Alexandria University, Alexandria, Egypt*
[d]*Department of Pharmaceutical Medicinal Chemistry and Drug Design, Faculty of Pharmacy (Girls), Al-Azhar University, Cairo 11754, Egypt*
[e]*Chemistry Department, College of Science at Yanbu, Taibah University, Yanbu 46423, Saudi Arabia*
[f]*Chemistry Department, College of Sciences, Taibah University, Al-Madina 30002, Saudi Arabia*
[g]*Medical Biotechnology Department, Genetic Engineering and Biotechnology Research Institute, City of Scientific Research and Technological Applications (SRTA-City), Egypt*

† Electronic supplementary information (ESI) available. See DOI: https://doi.org/10.1039/d4ra02222j

controlling the tumor microenvironment by attracting inflammatory cells and promoting angiogenesis.[12] Furthermore, therapeutic response and metastasis are strongly influenced by the EGFR/PI3K/AKT/mTOR signaling.[13,14] It should come as no surprise that the signaling pathway is frequently elevated in a range of human malignancies, given its complex roles in carcinogenesis.[15,16] Combination techniques within the EGFR–PI3K–mTOR pathways may be a useful strategy to increase therapeutic efficacy when some tumor subclones develop resistance to a single treatment due to genetic alterations as well. When treating tumors connected to these changes, targeting different parts of the EGFR–PI3K–mTOR axis may prove to be an effective treatment strategy.[17]

In response to stress, the p53 protein acts like a conductor in a complex cellular orchestra. It controls the activity of several genes (PTEN, IGF-BP3, TSC2, and AMPKb) that act as brakes on important growth signals (Akt and mTOR). This slows down cell division and helps reverse the characteristics of cancer cells. Additionally, p53 working with LKB1 further restricts cell proliferation. But that's not all! p53 also activates a cellular recycling process called autophagy, which helps stressed cells survive.[18]

The literature made it evident that 1,2,3-triazole derivatives containing 1,2,4-oxadiazole and 1,3-oxazole, **Ia** and **Ib**, showed encouraging cytotoxicity against the epithelial cancer cell line A549 (lung cancer), with IC_{50} values of 0.79 and 0.19 μM, respectively, while etoposide, the drug used as a reference, showed IC_{50} value of 3.08 mM.[19] When tested against A549, a library of 1,2,4-oxadiazole that included 1,2,3-triazoles, compound **II**[20] showed strong anticancer activity (IC_{50} 0.45 ± 0.023 μM). Furthermore, compound **III** was found to have a high and selective ant proliferative capability in A549 cells, with an IC_{50} value of 0.07 μM. It was also reported to raise the populations of early and late apoptotic/primary necrotic cells by 26.97% and 16.37%, respectively.[21] The hybrid **IV** containing a 4-bromophenyl-thiazole moiety, exhibited potent antiproliferative activity on the same cell line, A-549, (IC_{50} 0.40 μM). When it's EGFR suppressing effect (IC_{50} 0.16 ± 0.05 μM) was compared to erlotinib (IC_{50} 0.08 ± 0.04 μM), the hybrid was shown to be remarkably effective (Fig. 1).[22]

As Fig. 2 shows, a few pharmacophoric properties of EGFR inhibitors are required for good affinity against the EGFR ATP binding site. The above features include: (1) a hydrophobic head that fits into a pocket (region I) and interacts with an amino acid Glu738; (2) a central flat aromatic heterocyclic moiety that sits comfortably within a pocket called adenine binding pocket allowing interactions with amino acids Met769, Leu768, Thr766, and Gln767; (3) solvent accessible area; and (4) hydrophobic pocket II. As lapatinib's analogues, two series of EGFRI were created *via* ligand-based drug design. As can be seen in Fig. 2, the terminal phenyl/benzyl (hydrophobic I) was planned to function as an equivalent for the chlorophenyl of lapatinib, and the middle flat aromatic heterocyclic moiety was designed to be 1,2,4-isoxazole, an isostere of pyrimidine to accommodate within the adenine binding pocket. The phenyl ring (partially structured quinazoline) will be represented by the central phenyl (hydrophobic II). Finally, lapatinib replaces furan with a side chain through the 1,2,3-triazole linked to the solvent accessible area. In order to maximise the pharmacokinetic characteristics of various aliphatic or aromatic side chains, substituent variation was also pursued (*R*).

2. Results and discussions

2.1. Chemistry

A new library of 3,5-diaryl-1,2,4-oxadiazoles[23] was designed and synthesized using the 3-benzyl/phenyl derivative of 5-(2-hydroxyphenyl-1,2,4-oxadiazole) (**1a** and **1b**) as starting materials. The primary method for creating 1,2,3-triazoles is the azide–alkyne cyclo-addition reaction.[24,25] As a result, the alkylation reaction of the starting materials **1a** and **1b** using propargyl bromide,[26] **2** produced the derivatives **3a** and **3b** of *O*-alkynyl oxadiazole. Moreover, compounds **3a** and **3b** were used as starting materials to create a library of target compounds as

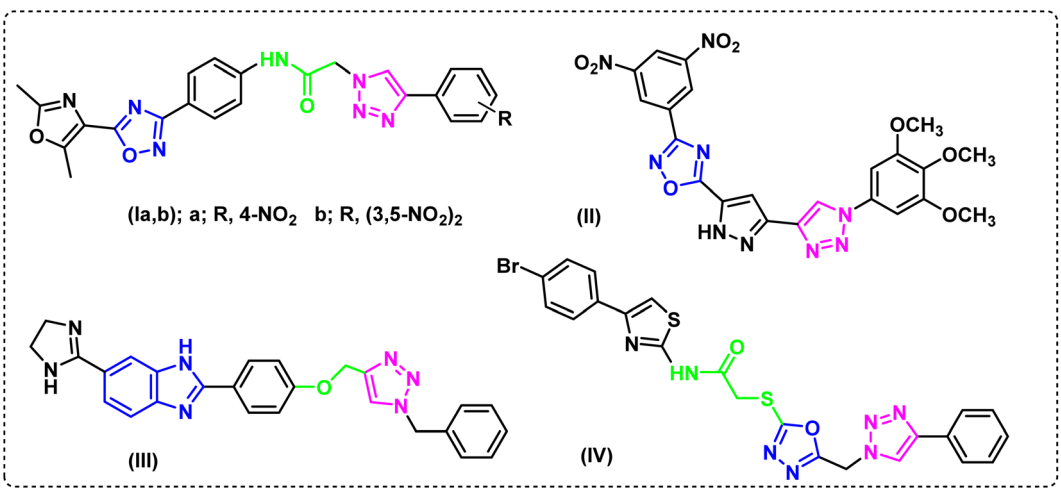

Fig. 1 Reported anticancer compounds.

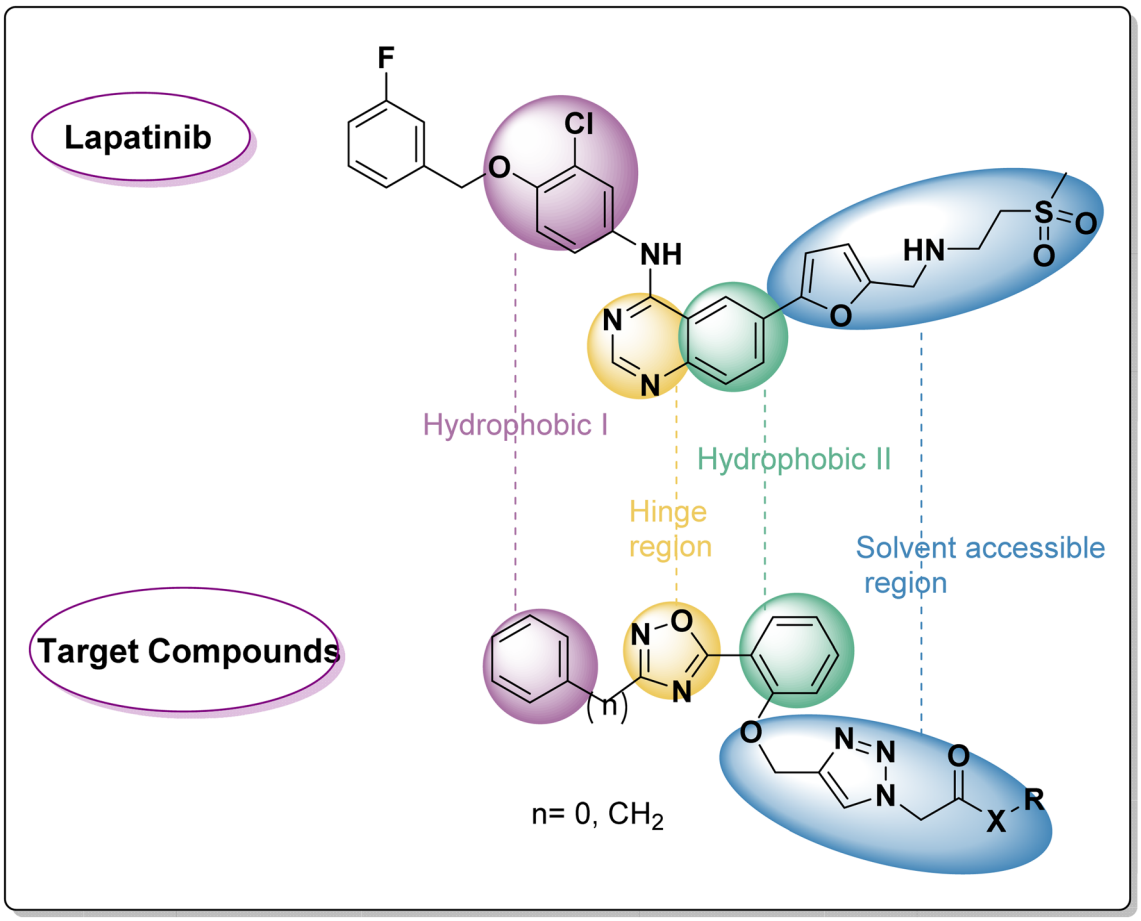

Fig. 2 Rational of target compounds.

quinoxaline triazole hybrids using the click reaction with ethyl 4-azidobenzoate, $Cu(OAc)_2$, and ascorbate[27] (Scheme 1). This method produced the corresponding quinoxaline-triazole esters, **5a** and **5b**, which were then treated with hydrochloric acid to produce their benzoic acid counterparts, **7a** and **7b**. Moreover, ammonolysis produced the acetamide analogues (**6a** and **6b**) of the esters **5a** and **5b** upon the introduction of ammonium hydroxide. Furthermore, the reaction of **5a** and **5b** with hydrazine hydrate in ethanol resulted in the production of the acetohydrazides **8a** and **8b** (Scheme 1). FT-IR, ^{1}H-NMR, ^{13}C-NMR and microanalytical analysis, were employed to validate the structure of the compounds (**5–11**). The spectroscopy findings supported the estimated structures. IR of compounds **5–8** confirmed the successful transformation of the ester group of compounds **5** into other functionalities such as amide, carboxy or hydrazide group corresponding to compounds **6**, **7**, and **8** respectively. Compound **6** showed C=O stretching near $\approx$1680 cm^{-1} rather than 1742 cm^{-1} that appeared for the ester functionality of **5**. Moreover, IR spectrum of **6** exhibited two absorption bands at $\approx$3310 and $\approx$3185 cm^{-1} that can be ascribed to the typically observed absorption for N–H stretching of NH_2 group. Furthermore, the carboxy group of compound **7** revealed a broad absorption peak in the region $\approx$3450–3300 cm^{-1} that is the usual OH stretching, in addition to carbonyl stretching at $\approx$1730 cm^{-1}. Compound **8** displayed the carbonyl stretching absorption band at $\approx$1660 cm^{-1} and also showed three absorption bands in the region 3350–3100 cm^{-1} which can be recognized to stretching bands of N–H and NH_2 groups.

The corresponding Schiff's bases, **9a** and **9b**, were obtained by condensing the acetohydrazide derivatives **8a** and **8b** with salicylaldehyde, as implemented in Scheme 2. Additionally, the imine derivatives **10a** and **10b** were made by refluxing **8a** and **8b** with pyridoxal-5′-phosphate monosodium salt (P5P)[28] in 100% ethanol. Ultimately, compounds **11a** and **11b** were produced by the neucleophilic addition of phenyl isothiocyanate to the acetohydrazide derivatives **8a** and **8b**. Schiff bases **9**, **10** have been derived from **8** *via* its condensation reaction with either salicylaldehyde or pyridoxal 5 phosphate (P5P). Their IR spectra showed appearance of an absorption band at $\approx$1600 cm^{-1} that

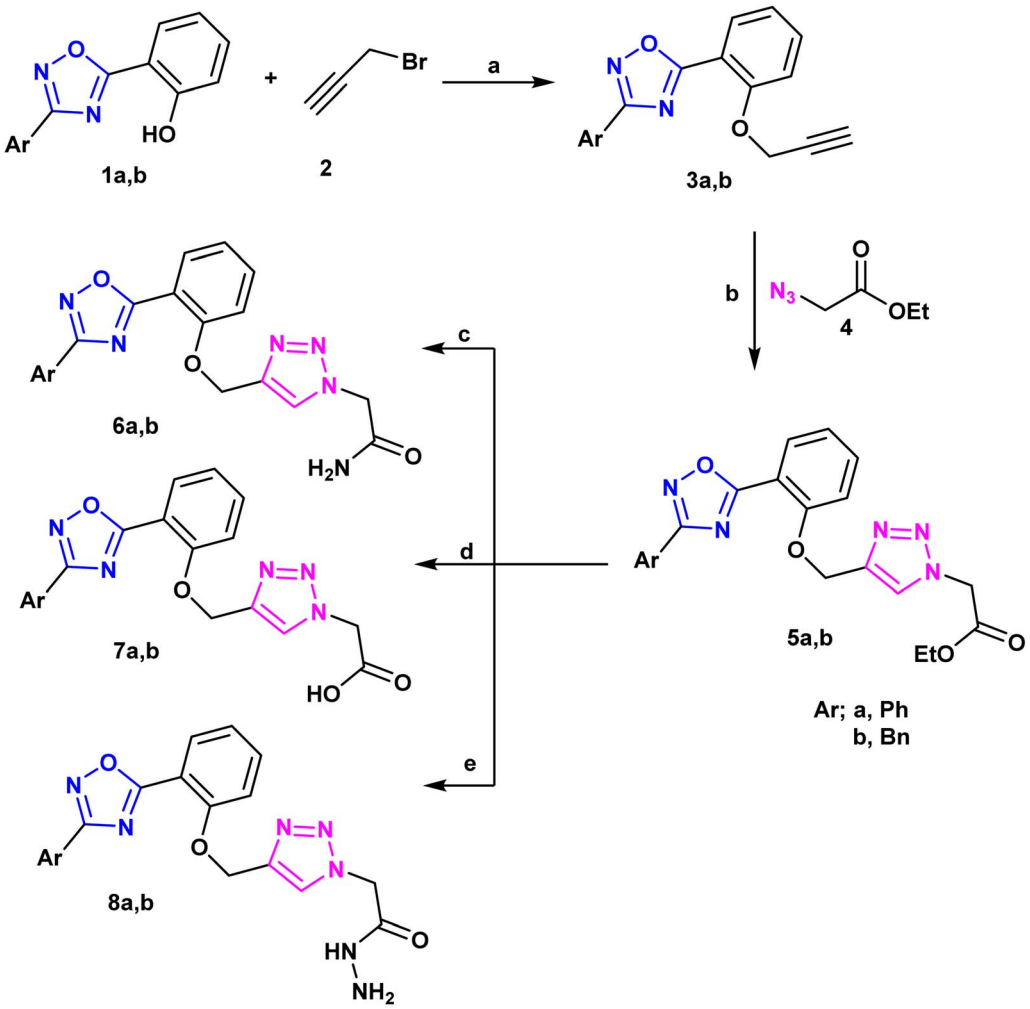

Scheme 1 Synthesis of hybrids 1,2,4-oxadizolel1,2,4-trazole derivatives. Reagents and conditions: (a); K_2CO_3, acetone, reflux 8 h, (b); $Cu(OAc)_2$, ascorbic acid, THF, r.t., reflux 16 h, (c); NH_4OH, r.t., reflux 16 h, (d); THF/H_2O (1:1) NaOH, pH =2; (e); $EtOH/N_2H_2$, reflux 4 h.

matches the imine (C=N) stretching. Moreover, their ^{1}H-NMR spectra showed a highly deshielded singlet at ≈8.6 ppm that corresponds to the azomethine proton (CH=N), which confirm the success of the condensation reaction. Additionally, ^{1}H-NMR of compounds **5–11** exhibited a singlet signal in the region ≈8.14–8.40 ppm that have been ascribed to the triazolyl proton[29] which validate the accomplishment of the copper-catalyzed azide–alkyne cycloaddition between compounds **3** and **4**. Both ^{1}H-NMR, ^{13}C-NMR spectroscopy confirmed that compounds **5–11** had the expected aliphatic proton and carbons respectively. The methylene and methyl groups showed signals between 1.16 and 5.70 ppm in the proton NMR spectrum, while; in the carbon NMR spectrum, the corresponding carbons of these aliphatic groups produced signals between 14.5 and 67 ppm. Additionally, both the proton and carbon NMR spectra confirmed the presence of aromatic rings. Consequently, aromatic protons displayed downfield peaks in ^{1}H-NMR at the region ≈7.00 to 8.10 ppm. Acidic protons (OH, NH, and NH_2) of compounds **6–11** exhibited broad signals in ^{1}H-NMR spectra and were characterized on the basis of their exchange by D_2O. Furthermore, ^{13}CNMR of compound **11** displayed a downfield signal near ≈180 ppm that has been attributed to the doubly bonded carbon of the thiocarbonyl group (C=S).

2.2. Biological evaluation

2.2.1. Determination of anticancer activity on breast (A549), colorectal cancer cell line (Caco-2). The MTT assay[30] was implemented to assess the antiproliferative activity of the target compounds (**5–11**) on lung cancer (A549) and colorectal cancer cells (Caco-2). Generally, most of them showed promising anticancer activity, (Table 1). Appealingly, compounds **6b**, **5a** exhibited very strong cytotoxicity against lung cancer IC_{50} 3.56 and 7.40 μM respectively. In addition, **8b**, **9a** and **9b** demonstrated very strong anticancer activity against both types of cancers; they displayed IC50 4.27, 6.52 and 2.51 toward A549 cell line and IC50 4.44, 3.37 and 2.89 μM against Caco-2 cell line respectively. Moreover, the target compound **5b** showed strong

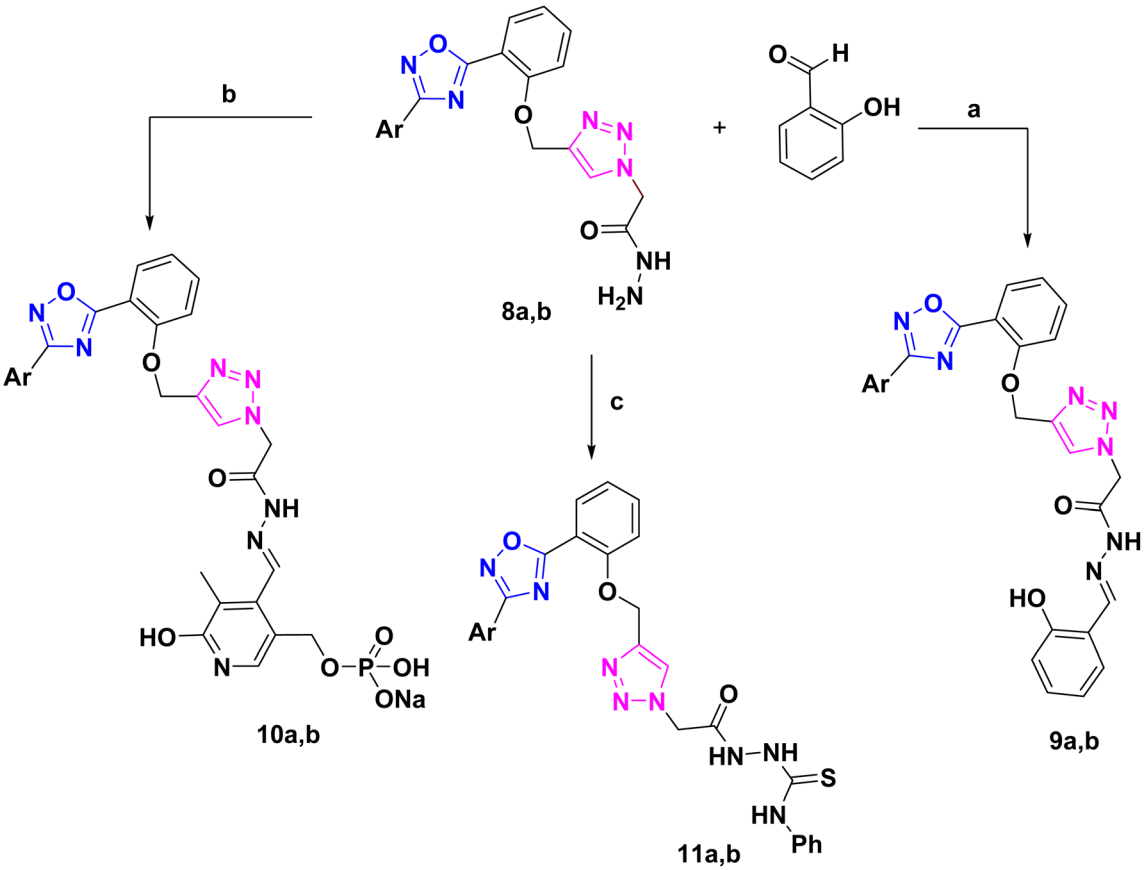

Scheme 2 Synthsis of Schiff's bases and thiourea derivatives based 1,2,4-oxadiazole. Reagents and conditions: (a), EtOH reflux 8 h, (b); P5P, EtOH, reflux 8h, (c); PhNCS, EtOH, reflux 8 h.

Table 1 IC_{50}s of the test compounds against A549, CaCo-2 and WI38

Compd no.	WI38	A549	SI	CaCo-2	SI
5a	14.27	7.40	1.93	26.31	0.54
5b	19.54	10.47	1.87	47.69	0.41
6a	29.78	12.73	2.34	14.09	2.11
6b	15.89	3.56	4.46	11.53	1.38
7a	22.38	210.2	0.11	98.11	0.23
7b	83.83	86.03	0.97	173.32	0.48
8a	30.63	13.09	2.34	12.89	2.38
8b	3.60	4.27	0.84	4.44	0.81
9a	6.10	6.52	0.93	3.37	1.81
9b	2.12	2.51	0.84	2.89	0.73
10a	9.02	29.50	0.31	26.71	0.34
10b	32.80	37.31	0.88	44.50	0.74
11a	21.59	12.37	1.75	32.18	0.67
11b	34.02	10.33	3.29	16.38	2.08
Doxorubicin	4.32	1.0	4.32	1.3	3.32

antiproliferative effect against lung cancer (IC_{50} 10.47 μM) while both **6a** (IC_{50}s 12.73 and 14.09 μM) and **11b** (IC_{50} 10.33 and 16.38 μM) exhibited strong cytotoxicity toward A549 and Caco-2 respectively. Another target compounds like **6b** displayed strong activity against Caco-2 cell line (IC_{50} 11.53 μM) while **11a** demonstrated strong activity toward A549 cell line (IC_{50} 12.37 μM). Additionally, moderate cytotoxicity was exhibited by **10a** and **10b** on the two cell lines. Similarly, **5a**, **5b**, and **11a** were in the moderate range of anticancer activity on Caco-2 cell line. Finally compounds **7a** and **7b** demonstrated weak to inactive cytotoxic level.

Noticeably, when comparing the cytotoxicity of the following pairs of compounds (**6a**, **6b**), (**8a**, **8b**), (**9a**, **9b**) and (**11a**, **11b**), their benzyl derivatives **6b**, **8b**, **9b** and **11b** were superior in activity than their phenyl analogs **6a**, **8a**, **9a** and **11a** which may be attributed to +I effect of the benzyl substituents.

2.2.2. Determination of anticancer activity on normal lung fibroblast (WI38). All compounds were tested for selective and safe cytotoxic activities against normal cell line WI38 compared to DOX employing MTT assay.[30] Most of the target compounds showed safety profile (IC_{50} 14.27–83.83 μM). Conversely, the cytotoxicity profiles of **8b**, **9a** and **9b** on lung and colon cell lines were comparable to that of doxorubicin, although they did not fall within a safe range (SI 0.73–0.93). Nonetheless, we compromised between selectivity index and cytotoxicity, for example, we chose the substances that showed strong anticancer activity along with excellent selectivity for further mechanistic study. Obviously, compounds **6a**, **6b**, **8a** and **11b**

Table 2 Effect of test compounds on the fold change of PI3K, mTOR, EGFR and P53

	A549				Caco-2			
Compd no.	PI3K	mTOR	EGFR	P53	PI3K	mTOR	EGFR	p53
Cancer	1 ± 0.0003	1 ± 0.004	1 ± 0.003	1 ± 0.007	1 ± 0.008	1 ± 0.001	1 ± 0.005	1 ± 0.01
6a	0.28 ± 0.002	0.27 ± 0.01	0.25 ± 0.007	6.5 ± 0.05	0.45 ± 0.001	0.35 ± 0.005	0.37 ± 0.08	4.75 ± 0.03
6b	0.24 ± 0.03	0.25 ± 0.0008	0.23 ± 0.004	5.9 ± 0.04	ND	ND	ND	ND
8a	0.3 ± 0.004	0.28 ± 0.009	0.26 ± 0.03	5.5 ± 0.003	0.43 ± 0.02	0.32 ± 0.09	0.35 ± 0.03	5.13 ± 0.02
11b	0.36 ± 0.005	0.31 ± 0.04	0.29 ± 0.08	5.4 ± 0.01	0.53 ± 0.0004	0.365 ± 0.01	0.423 ± 0.005	4.36 ± 0.05
Doxorubicin	0.1 ± 0.008	0.18 ± 0.07	0.16 ± 0.02	8.3 ± 0.02	0.19 ± 0.003	0.16 ± 0.002	0.15 ± 0.03	7.9 ± 0.03

were acknowledged as the most active and selective derivatives among the series (Table 1).

2.2.3. Mechanistic study. The potent cytotoxic compounds **6a**, **6b**, **8a** and **11b** were selected for examination by real-time PCR analyses to explore their effects on PI3K, mTOR, EGFR and p53[31–34] pathway using B-actin as a housekeeping gene. Table 2 shows the data as fold change values where A549 was more sensitive to our compounds than Caco-2 cell line. Generally, on A549 cell line, our hits can suppress gene expression of PI3K by 0.24–0.36 fold, downstream gene EGFR by 0.23–0.29 fold; and down regulate mTOR by 0.25–0.31 folds. Nicknamed the "guardian of the genome", the p53 gene is a crucial tumor suppressor. Unfortunately, in over half of all human cancers, this gene gets mutated. When p53 functions normally, it acts like a brake on cell growth, preventing tumors from forming. Conversely to the action on previous oncoenes, they up regulate p53 by 5.4–6.5 folds. Parallel results for these genes on Caco-2, but the results on A549 were slightly better. The results on lung cancer cell line (A549) revealed that, 6b displayed the highest potential to suppress PI3K/mTOR/EGFR while **6a** showed the best potential to induce apoptosis *via* upregulation of p53. Concerning the results on colon cancer (Caco-2) cell line, **8a** showed the highest tendency either to suppress the oncogenic mediators PI3K/mTOR/EGFR or to upregulate p53 by 5.13 folds.

A correlation between downregulation of PI3K, mTOR and EGFR and upregulation of p53 expression was evident, thus the activity order of our hits towards the tested oncogenic mediators was **6b** > **6a** > **8a** > **11b** (Table 2 and Fig. 3–5).

2.2.4. *In silico* assessment of ADME and physicochemical characteristics. The physicochemical and ADME properties of the synthesised compounds were assessed by a computer analysis. Using software called SwissADME,[35] it was possible to determine whether the compounds were likely to be bioactive based on a number of important factors, including the Veber and Lipinski rules. Table 3 illustrates that the physicochemical characteristics of the majority of test compounds align with the Lipinski and Veber criteria, exhibiting zero violation.[36,37] This suggests that the derivatives exhibit promising drug-like qualities. According to Lipinski's rule of five, all compounds have no more than one violation of these conditions; therefore they are predicted to be orally active drug candidates except **10a** and **10b**.

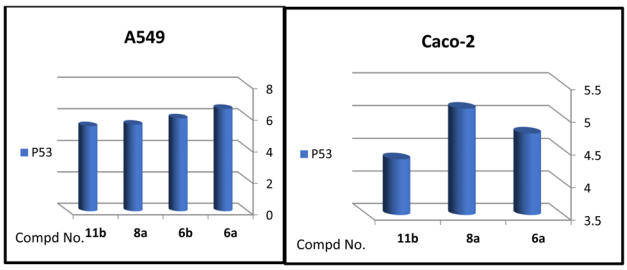

Fig. 5 Effect of test compounds on the fold change of p53 in A549 and Caco-2 cell lines.

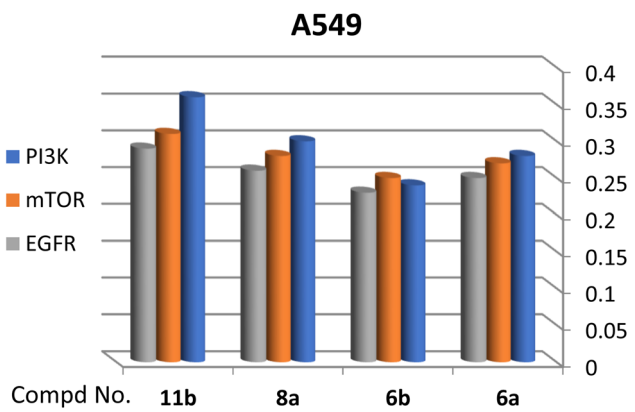

Fig. 3 Effect of test compounds on the fold change of PI3K, mTOR, EGFR in A549 cell line.

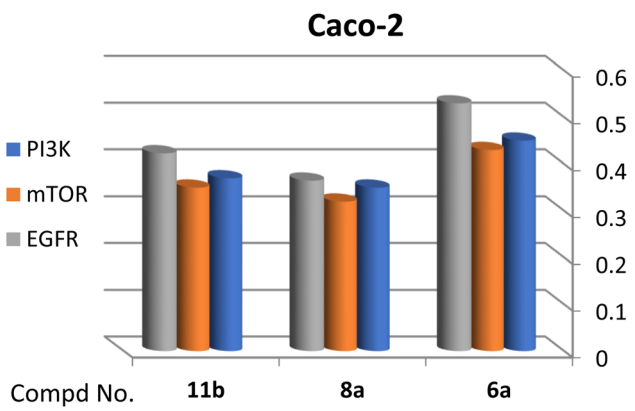

Fig. 4 Effect of test compounds on the fold change of PI3K, mTOR, EGFR in Caco-2 cell line.

Table 3 The number of rotatable bonds and the physicochemical characteristics based on Lipinski's rule of five

Compd no.	HBD	HBA	*M* log *P*	M. Wt	No. of rot. bonds	Lipinski's violations	Veber's violations
5a	0	8	2.18	421.45	9	0	0
5b	0	8	2.12	435.48	10	0	0
6a	1	7	1.10	376.37	7	0	0
6b	1	7	1.06	390.40	8	0	0
7a	1	8	1.51	377.35	7	0	0
7b	1	8	1.47	391.38	8	0	0
8a	2	8	1.14	391.38	8	0	0
8b	2	8	1.10	405.41	9	0	0
9a	2	9	2.08	511.53	10	1	1
9b	2	9	2.02	525.56	11	1	1
10a	4	14	1.96	620.51	13	2	2
10b	4	14	0.26	634.54	14	2	2
11a	4	8	1.53	544.58	12	1	2
11b	4	8	1.47	558.61	13	1	2
Erlotinib	1	6	1.89	393.44	10	0	0

Table 4 The % ABS and the topological polar surface area (TPSA)

Cpd. no.	TPSA	% ABS
5a	105.16	72.72
5b	105.16	72.72
6a	121.95	66.93
6b	121.95	66.93
7a	116.16	68.92
7b	116.16	68.92
8a	133.98	62.78
8b	133.98	62.78
9a	140.55	60.51
9b	140.55	60.51
10a	230.01	29.65
10b	230.01	29.65
11a	173.34	49.20
11b	173.34	49.20
Erlotinib	74.73	83.22

As adopted in Table 4, it is well established that the topological polar surface area (TPSA)[38] is a trustworthy indicator of intestinal medication absorption (TPSA less than 140 Å^2) and drug penetration through the blood–brain barrier (TPSA less than 60 Å^2). All compounds, with the exception of **9–11**, satisfy Veber's rule since their computed TPSA values fall within the range that allows them to pass through cell membranes. Additionally, absorption (% ABS) was computed using the formula % ABS = 109 − (0.345 × TPSA). The results showed that the calculated % ABS of all these hits varied from 60.51% to 72.72%, suggesting that these synthetic derivatives—aside from compounds **10** and **11**—may have the required bioavailability and cell membrane permeability (Table 4).

Additionally, the test compounds' medicinal chemistry properties and drug-likeness were predicted using the SwissADME software (Table 5). With the exception of compounds **9–11**, all compounds have high GI absorption and high bioavailability ratings (0.55). For the majority of substances, the SwissADME also forecasted no alerts. Furthermore, according to a study by SwissADME, all of the analogues had synthetic accessibility scores ranging from 3.43 to 4.74, meaning that they could all be readily synthesised on a large scale and were on par with the reference drug, erlotinib (3.19).

It's interesting to note that our hits, which are systemically targeted compounds, will have little to no central nervous system side effects because they do not penetrate the blood–brain barrier, an advantage over erlotinib. With the exception of compounds **7a** and **7b**, the majority of our novel compounds are P-gp substrates. All things considered, it was possible to determine that our hits had drug-likeness values and medicinal chemistry criteria that were appropriate, indicating that they might be considered as potential drugs.

2.2.5. Molecular docking study. Understanding the binding mechanism between novel compounds and their targets is crucial for lead discovery investigations and future optimization. Consequently, compounds **6a**, **6b**, **8a** and **11b** were subjected to docking analysis within the specified active site of EGFR. X-ray structure of EGFR combined with gefitinib was obtained from the Protein Data Bank with the ID number 2ITY. Docking validation included re-docking the co-crystalized ligand (gefitinib) into the pre-determined active site resulted in an RMSD value of 0.83 Å and a docking score of −5.84 kcal mol^{-1}.

The investigation of the binding mode between gefitinib and the EGFR active site showed the crucial hydrogen bond interaction with the important residue Met793 in the hinge region. The moiety of 3-chloro-4-fluoroaniline expanded into the hydrophobic pocket I located at the back of the ATP-binding site forming hydrophobic interactions with the Val726, Lys745, and Leu788 residues. In addition, the quinazoline and the methoxy substituent were in hydrophobic contacts with Leu718, Ala743, and Pro794 residues. On the other hand, the propylmorpholine moiety was extended in the solvent region forming electrostatic and carbon–hydrogen bond interactions with Asp800 (Fig. 6).

Table 5 Medicinal chemistry and pharmacokinetic parameters

Cpd. no.	GI absorption	BBB permeation	P-gp substrate	Bioavailability score	Pains alerts	Synthetic accessibility
5a	High	No	Yes	0.55	0	3.86
5b	High	No	Yes	0.55	0	3.95
6a	High	No	Yes	0.55	0	3.43
6b	High	No	Yes	0.55	0	3.53
7a	High	No	No	0.56	0	3.43
7b	High	No	No	0.56	0	3.52
8a	High	No	Yes	0.55	0	3.57
8b	High	No	Yes	0.55	0	3.67
9a	Low	No	Yes	0.17	1	4.37
9b	Low	No	Yes	0.17	1	4.46
10a	Low	No	Yes	0.11	0	4.63
10b	Low	No	Yes	0.11	0	4.74
11a	Low	No	Yes	0.17	0	4.25
11b	Low	No	Yes	0.17	0	4.35
Erlotinib	High	Yes	No	0.55	0	3.19

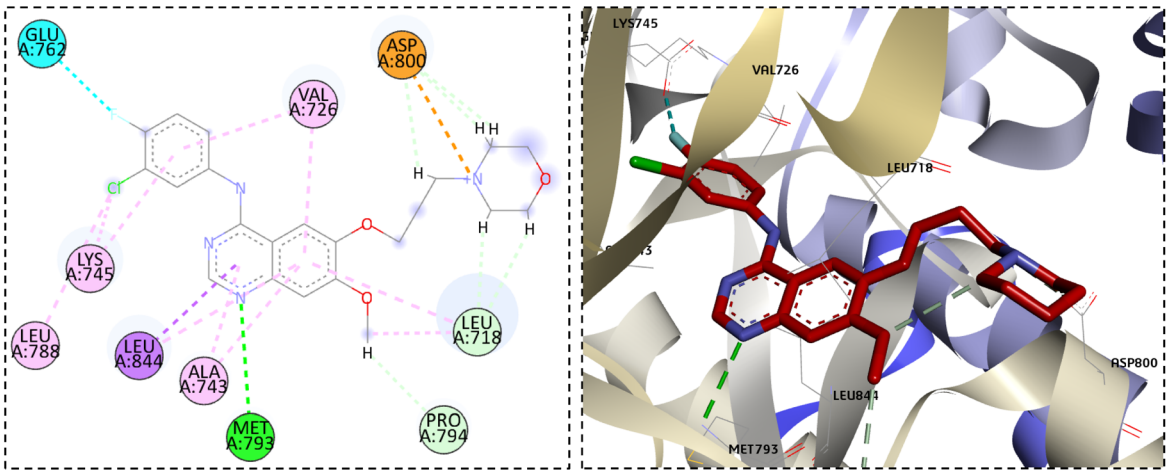

Fig. 6 The docked pose of gefitinib in the EGFR active site.

Interestingly, when the new compounds (**6a**, **6b**, **8a**, and **11b**) docked to EGFR, they produced a favourable binding through a binding pattern close to that of gefitinib, yielding docking scores of −6.85, −7.04, −7.49, and −7.91 kcal mol^{-1}, respectively. The oxadiazole ring of the docked derivatives was oriented in the hinge region, with its oxygen atom acting as a hydrogen bond acceptor for the key amino acid Met793, in addition to hydrophobic interactions with Val726, Ala743, and Leu844 residues. The terminal phenyl group of these compounds was positioned in the back hydrophobic pocket, forming non polar interactions with the Val726 and Lys745 residues, while the phenyl ring at the 5 position of the oxadiazole ring occupied the hydrophobic pocket II, interacting with Leu718 through a Pi-alkyl or Pi-sigma interaction. Finally, the substituted triazolyl moiety expanded near the solvent area (Fig. 7). The triazolylacetamide motif of compound **6a** was found to be rotated towards the hydrophobic pocket I, forming carbon–hydrogen bond with Gly719 and a hydrophobic interaction with Val726. As well, the acetohydrazide group of **8a** and the N-phenylhydrazine-1-carbothioamide moiety of **11b** were rotated close to Asp855 side chain, forming an electrostatic interaction. However, the acetamide group of compound **6b** showed a different orientation in which it was extended near Cys797 and Asp800 at the edge of the active site, forming H-bonds with them (Fig. 7). Overlay of the reference drug gefitinib and the new target compounds **6a**, **6b**, **8a**, and **11b** in the EGFR active site is shown in Fig. 8.

2.2.6. Statistical Analysis.[39] All data were expressed as mean ± standard deviation (SD). The differences were statistically significant at $P < 0.05$. Statistical analyses were carried out using

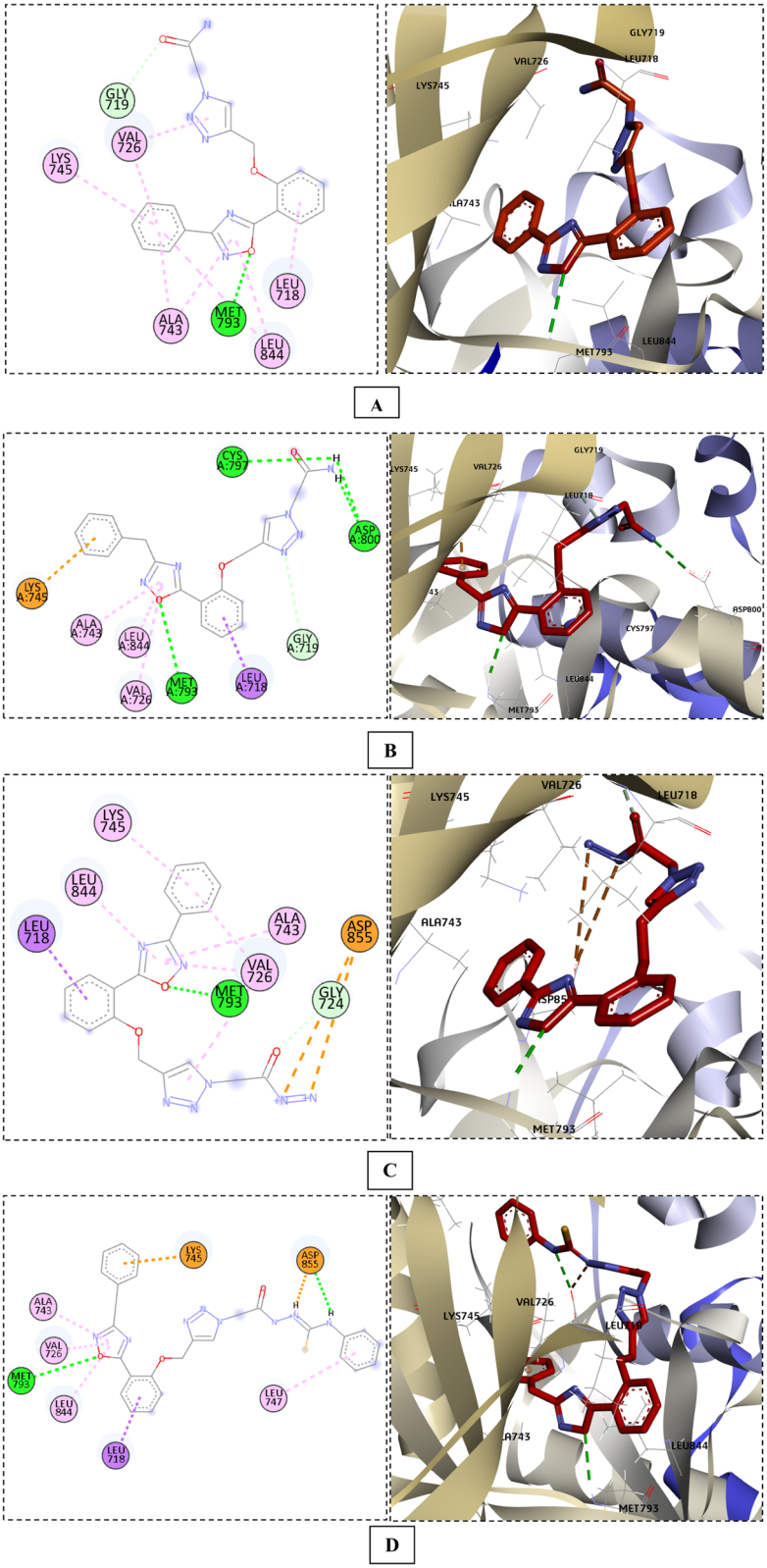

Fig. 7 The docking poses of compounds **6a** (A), **6b** (B), **8a** (C), and **11b** (D) in the EGFR active site.

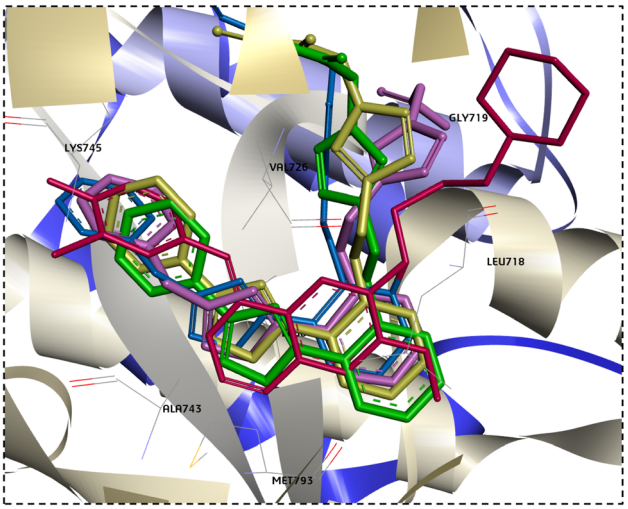

Fig. 8 Overlay docking alignment of gefitinib (red), **6a** (green), **6b** (purple), **8a** (yellow), and **11b** (blue) in the active site of EGFR.

Table 6 Sequence of primers for mutational analysis of PI3K, mTOR, EGFR, and p53 genes

PI3K	Forward: 5′-CTG CCTGCG ACAGATGAG TG-3 Reverse: 5′-TCCGAT TACCAAGTG CTC TTTC-3
mTOR	Forward: 5′-ACA ACT TTG GTATCG TGG AAGG-3′ Reverse: 5′-GCC ATC ACG CCACAG TTTC-3′
EGFR	Forward: 5′-TGGAGC TACGGG GTGACCGT-3 Reverse: 5′-GGT TCAGAG GCT GAT TGT GAT-3
p53	Forward: CCTCAGCATCTTATCCGAGTGG Reverse: TGGATGGTGGTACAGTCAGAGC
B-actin	Forward: 5′-TCA AGA AGG TGG TGA AGC AGG-3′ Reverse: 5′-AGCGTC AAAGGTGGAGGAGTG-3′

primers of Biostatistics program V5 for analysis of unpaired Student *t*- Test and one way (ANOVA).

3. Conclusions

We synthesized and examined the anticancer properties of fourteen 1,2,4-oxadiazole tethered 1,2,3-triazole derivatives. The MTT assay was used to assess the cytotoxicity of these drugs against A549, Caco-2, and WI38 cell lines, with doxorubicin serving as the reference standard. Potent and specific cytotoxicity against lung cancer (A549) and colon cancer (Caco-2) was demonstrated by four compounds: **6a**, **6b**, **8a**, and **11b**. It was looked into how they affected the PI3K/mTOR/EGFR pathway. The promising hits showed significant fold changes in the downregulation of EGFR, mTOR, and PI3K, according to qPCR data. Moreover, they upregulate the amount of p53, supporting their mechanism of action. Furthermore, our compounds may be considered safe drug-like candidates based on their physicochemical and drug-likeness findings.

It is feasible to conclude from the findings of this investigation that the freshly synthesized compounds have the potential to be a novel class of anticancer drugs for lung and colon tumors, and this warrants further exploration based on the study's findings.

4. Experimental

4.1. Chemistry

4.1.1. General methodology for click reaction for synthesis of 5a and 5b. A suspension of $Cu(OAc)_2$ (20 mol%) and ascorbic acid (40 mol%) in H_2O (2 mL) was added to a solution of ethyl-2-azidoacetate (**4**) (50 mg, 0.38 mmol), and 3-aryl-5-(2-(prop-2-yn-1-yloxy)phenyl)-1,2,4-oxadiazole (**3a** or **3b**) (0.36 mmol) in THF (4 mL), and the reaction was stirred for 16 h at room temperature, diluted with H_2O (10 mL) and the product was extracted into ethyl acetate (3 × 30 mL). The combined extracts were washed with aqueous $NaHCO_3$ followed by brine and then dried (Na_2SO_4). The solvent was removed and the product purified over silica gel eluting with ethyl acetate/petrol (5 : 1).

*4.1.1.1 Ethyl 2-(4-((2-(3-phenyl-1,2,4-oxadiazol-5-yl)phenoxy) methyl)-1H-1,2,3-triazol-1-yl)acetate (**5a**).* To afford **5a** as a white solid (72% yield): m.p = 102–104 °C; R_f = 0.53 (EtOAc: *n*-hexane, 1 : 2); IR (KBr) ν_{max}/(cm^{-1}): 1749 (CO, ester). ^{1}H NMR (500 MHz, DMSO-d_6) δ_H: 8.26 (s, 1*H*, Triazole–H), 8.08–8.02 (m, 3*H*, Ar–H), 7.67 (t, J = 8.5 Hz, 1*H*, Ar–H), 7.59–7.51 (m, 4*H*, Ar–H), 7.18 (t, J = 7.5 Hz, 1*H*, Ar–H), 5.4 (d, J = 4.5 Hz, 4*H*, O–CH_2, N–CH_2), 4.13 (q, 2*H*, CH_2), 1.16 (t, J = 7.0 Hz, 3*H*, CH_3), ^{13}C NMR (125 MHz, DMSO-d_6) δ_C: 175.5, 168.1, 167.7, 157.4, 143.0, 135.3, 132.1, 131.9, 129.8, 127.6, 126.8, 126.6, 121.9, 114.9, 113.2, 62.7, 62.0, 51.0, 14.5. Anal. calcd for $C_{21}H_{19}N_5O_4$ (M. wt: 405.41): C, 62.22; H, 4.72; N, 17.27; found: C, 62.43; H, 4.89; N, 17.51.

*4.1.1.2 Ethyl 2-(4-((2-(3-benzyl-1,2,4-oxadiazol-5-yl)phenoxy) methyl)-1H-1,2,3-triazol-1-yl)acetate (**5b**).* To afford **5b** as a white solid (75% yield) m.p = 114–116 °C; R_f = 0.53 (EtOAc: *n*-hexane, 1 : 2); IR (KBr) ν_{max}/(cm^{-1}): 1742 (CO, ester). ^{1}H NMR (500 MHz, DMSO-d_6) δ_H: 8.19 (s, 1*H*, Triazole–H), 7.92 (d, J = 9.5 Hz, 1*H*, Ar–H), 7.61 (t, J = 7.5 Hz, 1*H*, Ar–H), 7.47 (d, J = 8.0 Hz, 1*H*, Ar–H), 7.33–7.20 (m, 5*H*, Ar–H), 7.11 (t, J = 7.5 Hz, 1*H*, Ar–H), 5.37 (d, J = 16 Hz, 4*H*, N–CH_2, O–CH_2), 4.13 (q, 4*H*, CH_3–CH_2, Ph–CH_2), 1.16 (t, 7 Hz, 3*H*, CH_2–CH_3), ^{13}C NMR (125 MHz, DMSO-d_6) δ_C: 175.1, 169.7, 167.7, 157.3, 143.0, 136.4, 135.1, 131.8, 129.5, 129.1, 127.4, 126.5, 121.8, 114.8, 113.2, 62.6, 62.0, 50.9, 31.9, 14.5. Anal. calcd for $C_{22}H_{21}N_5O_4$ (M.wt: 419.43): C, 63.00; H, 5.05; N, 16.70; found: C, 63.24; H, 5.21; N, 16.93.

4.1.2. Synthesis of the acid amide 6a and 6b. A mixture of compound the ester (**5a** or **5b**) (0.14 mmol) in THF (2.5 mL) ammonium hydroxide (2.5 mL, 25%) was added dropwise to the reaction mixture with stirring for one hour. The reaction mixture was heated under reflux for 30 min., the resulting product that separated out was filtered off.

*4.1.2.1 2-(4-((2-(3-Phenyl-1,2,4-oxadiazol-5-yl)phenoxy) methyl)-1H-1,2,3-triazol-1-yl)acetamide (**6a**).* To afford compound **6a** as grey solid (76% yield); m.p = 148–150 °C; R_f = 0.32 (ethyl acetate: *n*-hexane: MeOH, 1 : 2: 0.5); IR (KBr): ν_{max}/(cm^{-1}): 3303, 3273 (NH_2), 1684 (OCN). ^{1}H NMR (500 MHz, DMSO-d_6) δ_H: 8.19 (s, 1H, Triazole–H), 8.08–8.03 (m, 3*H*, Ar–H), 7.75 (s, 1*H*, Ar–H), 7.67 (t, J = 7.5 Hz, 1*H*, Ar–H), 7.56–7.53 (m, 4*H*, Ar–H, NH_2), 7.39 (s, 1*H*, Ar–H), 7.18 (t, J = 7.5 Hz, 1*H*, Ar–H), 5.38 (s, 2*H*, O–CH_2), 5.08 (s, 2*H*, N–CH_2). ^{13}C NMR (125 MHz,

DMSO-d_6) δ_C: 175.4, 168.1, 167.8, 157.5, 142.6, 135.3, 132.1, 131.9, 129.8, 127.6, 126.8, 126.7, 121.9, 114.9, 113.2, 62.8, 52.0. Anal. Calcd for $C_{19}H_{16}N_6O_3$ (M. wt: 376.38): C, 60.63; H, 4.29; N, 22.33; found: C, 60.91; H, 4.45; N, 22.60.

*4.1.2.2 2-(4-((2-(3-Benzyl-1,2,4-oxadiazol-5-yl)phenoxy) methyl)-1H-1,2,3-triazol-1-yl)acetamide (**6b**).* To afford **6b** as grey solid (60% yield): m.p = 220–222 °C; R_f = 0.28 (ethyl acetate: *n*-hexane: methanol, 1 : 2: 0.5); IR (KBr) ν_{max}/(cm^{-1}): 3318, 3184 (NH_2), 1683 (OCN). ^{1}H NMR (500 MHz, DMSO-d_6) δ_H: 8.13 (s, 1*H*, Triazole-H), 7.92 (d, J = 6.5 Hz, 1*H*, Ar–H), 7.74 (s, 1*H*, Ar–H), 7.61 (t, J = 7.5 Hz, 1*H*, Ar–H), 7.48 (d, J = 9.0 Hz, 1*H*, Ar–H), 7.39 (s, 1*H*, Ar–H), 7.33–7.27 (m, 4*H*, Ar–H, NH_2), 7.23–7.20 (m, 1*H*, Ar–H), 7.10 (t, J = 7.5 Hz, 1*H*, Ar–H), 5.33 (s, 2*H*, N–CH_2), 5.06 (s, 2*H*, O–CH_2), 4.11 (S, 2*H*, Ph–CH_2). ^{13}C NMR (125 MHz, DMSO-d_6) δ_C: 175.1, 169.7, 167.8, 157.3, 142.6, 136.4, 135.1, 131.8, 129.5, 129.1, 127.4, 126.7, 121.8, 114.9, 113.2, 62.7, 52.0, 31.9. Anal. Calcd for $C_{20}H_{18}N_6O_3$ (M.wt: 390.40): C, 61.53; H, 4.65; N, 21.53; found: C, 61.80; H, 4.73; N, 21.68.

4.1.3. General methodology for synthesis of 7a and 7b. The saponification of the ester was accomplished by addition of the NaOH (1N, 10 mL) to **5a** or **5b** (0.25 mmol) then the reaction was stirred for 1 hour at room temperature. Finally, the reaction mixture was poured into water (100 mL) then acidify to pH = 2. The obtained desired precipitate was filter, washed with water and dried to give **7a** or **7b** respectively.

*4.1.3.1 2-(4-((2-(3-Phenyl-1,2,4-oxadiazol-5-yl)phenoxy) methyl)-1H-1,2,3-triazol-1-yl)acetic acid (**7a**).* As off-white powder (85% yield); m.p= 198–200 °C R_f = 0.53 (EtOAc: *n*-hexane, 1 : 2); IR (KBr) ν_{max}/(cm^{-1}): 3031 (OH, carboxyl), 1723 (CO, carboxyl). ^{1}H NMR (500 MHz, DMSO-d_6) δ_H: 13.42 (bs, 1*H*, OH), 8.24 (s, 1*H*, Triazole–H), 8.08–8.02 (m, 3*H*, Ar–H), 7.66 (t, J = 8.0 Hz, 1*H*, Ar–H), 7.57–7.51 (m, 4*H*, Ar–H), 7.17 (t, J = 7.5 Hz, 1*H*, Ar–H), 5.39 (s, 2*H*, O–CH_2), 5.29 (s, 2*H*, N–CH_2) ^{13}C NMR (125 MHz, DMSO-d_6) δ_C: 175.4, 169.2, 168.1, 157.4, 142.9, 135.3, 132.1, 131.9, 129.8, 127.6, 126.8, 126.5, 121.9, 114.9, 113.2, 62.8, 51.1. Anal. Calcd for $C_{19}H_{15}N_5O_4$ (M. wt: 377.35): C, 60.47; H, 4.01; N, 18.56; found: C, 60.70; H, 4.25; N, 18.82.

*4.1.3.2 2-(4-((2-(3-Benzyl-1,2,4-oxadiazol-5-yl)phenoxy) methyl)-1H-1,2,3-triazol-1-yl)acetic acid (**7b**).* As off-white powder (80% yield); m.p = 175–177 °C; R_f = 0.53 (EtOAc: *n*-hexane, 1 : 2); IR (KBr) ν_{max}/(cm^{-1}): 3456 (OH, carboxyl), 1735 (CO, carboxyl). ^{1}H NMR (500 MHz, DMSO-d_6) δ_H: 13.42 (bs, 1*H*, OH), 8.17 (s, 1*H*, Triazole–H), 7.92 (d, J = 9.5 Hz, 1*H*, Ar–H), 7.61 (t, J = 7.0 Hz, 1*H*, Ar–H), 7.48 (d, J = 8.0 Hz, 1*H*, Ar–H), 7.30–7.27 (m, 4*H*, Ar–H), 7.23–7.20 (m, 1*H*, Ar–H), 7.11 (t, J = 7.5 Hz, 1*H*, Ar–H), 5.34 (s, 2*H*, O–CH_2), 5.27 (s, 2*H*, N–CH_2), 4.11 (s, 2*H*, Ph–CH_2), ^{13}C NMR (125 MHz, DMSO-d_6) δ_C: 175.1, 169.7, 169.1, 157.3, 142.9, 136.4, 135.1, 131.8, 129.5, 129.1, 127.4, 126.5, 121.8, 114.9, 113.2, 62.7, 51.1, 31.9. Anal. Calcd for $C_{20}H_{17}N_5O_4$ (M. wt: 391.38): C, 61.38; H, 4.38; N, 17.89; found: C, 61.21; H, 4.49; N, 18.03.

4.1.4. Synthesis of the acid hydrazide 8a and 8b. A mixture of the ester **5a** or **5b** (1.2 mmol) and hydrazine hydrate (3.5 mL, 99%) in ethanol (10 mL) was refluxed for 1 h, then left to cool at room temperature. The resultant solid was filtered and crystalized from ethanol.

*4.1.4.1 2-(4-((2-(3-Phenyl-1,2,4-oxadiazol-5-yl)phenoxy) methyl)-1H-1,2,3-triazol-1-yl)acetohydrazide (**8a**).* To give **8a** off-white solid (64% yield): m.p = 194–196 °C; R_f = 0.53 (ethyl acetate: *n*-hexane, 3 : 1); IR (KBr) ν_{max}/(cm^{-1}): 3330, 3307 (NH_2), 3248 (NH), 1653 (OCN); ^{1}H NMR (500 MHz, DMSO-d_6) δ_H: 9.52 (bs, 1*H*, NH), 8.22 (s, 1*H*, Triazole–H), 8.08–8.03 (m, 3*H*, Ar–H), 7.67 (t, J = 7.5 Hz, 1*H*, Ar–H), 7.56–7.52 (m, 4*H*, Ar–H), 7.17 (t, J = 8.0 Hz, 1*H*, Ar–H), 5.38 (s, 2*H*, N–CH_2), 5.04 (s, 2*H*, O–CH_2), 4.56 (s, 1*H*, NH), 4.34 (bs, 1*H*, NH). ^{13}C NMR (125 MHz, DMSO-d_6) δ_C: 175.5, 168.1, 157.5, 142.7, 135.3, 132.1, 131.9, 129.8, 127.6, 126.9, 126.8, 126.6, 121.8, 114.9, 113.2, 62.7, 51.0. Anal. Calcd for $C_{19}H_{17}N_7O_3$ (M. wt: 391.39): C, 58.31; H, 4.38; N, 25.05; found: C, 58.47; H, 4.50; N, 24.97.

*4.1.4.2 2-(4-((2-(3-Benzyl-1,2,4-oxadiazol-5-yl)phenoxy) methyl)-1H-1,2,3-triazol-1-yl)acetohydrazide (**8b**).* To give **8b** white solid (72% yield): m.p = 223–225 °C; R_f = 0.53 (EtOAc: *n*-hexane, 1 : 2); IR (KBr) ν_{max}/(cm^{-1}): 3338, 3285 (NH_2), 3139 (NH), 1653 (OCN); ^{1}H NMR (500 MHz, DMSO-d_6) δ_H: 9.53 (bs, 1*H*, NH), 8.17 (s, 1*H*, Triazole–H), 7.92 (s, 1*H*, Ar–H), 7.61 (s, 1*H*, Ar–H), 7.48 (s, 1*H*, Ar–H), 7.40–7.20 (m, 5*H*, Ar–H), 7.10 (s, 1*H*, Ar–H), 5.33 (s, 2*H*, N–CH_2), 5.03 (s, 2*H*, O–CH_2), 4.55 (s, 1*H*, NH), 4.35 (s, 1*H*, NH), 4.11 (s, 2*H*, Ph–CH_2). ^{13}C NMR (125 MHz, DMSO-d_6) δ_C: 175.1, 169.7, 157.3, 142.7, 136.4, 135.1, 131.8, 129.5, 129.1, 127.4, 126.5, 121.8, 114.8, 113.2, 62.6, 51.0, 50.7, 31.9. Anal. Calcd for $C_{20}H_{19}N_7O_3$ (M. wt: 405.42): C, 59.25; H, 4.72; N, 24.18; found: C, 59.53; H, 4.91; N, 24.43.

4.1.5. General methedolgy for synthesis of Schiff's base 9a, 9b, 10a and 10b. To a stirred solution of the acid hydrazide **8a** or **8b** (0.12 mmol) in ethanol (10 mL), salicylaldehyde or pyridoxal-5-phosphate mono sodium salt (0.25 mmol) respectively was added and the reaction mixture was heated under reflux for 6 h, then left to cool at room temperature. The solid formed was filtered off.

*4.1.5.1 N′-(2-Hydroxybenzylidene)-2-(4-((2-(3-phenyl-1,2,4-oxadiazol-5-yl)phenoxy)methyl)-1H-1,2,3-triazol-1-yl) acetohydrazide (**9a**).* Recrystallized from ethanol to form white solid (78% yield); m.p = 212–214 °C; R_f = 0.53 (Ethyl Acetate: *n*-hexane, 3 : 1); IR (KBr) ν_{max}/(cm^{-1}): 3550 (OH), 3480 (NH), 1684 (OCN), 1604 (C=N). ^{1}H NMR (500 MHz, DMSO-d_6) δ_H: 11.76 (s, 1*H*, NH), 10.12 (s, 1*H*, OH), 8.44–8.21 (m, 2*H*, N=CH, Ar–H), 8.09–8.03 (m, 3*H*, Triazole–H, Ar–H), 7.75 (d, J = 7.5 Hz, 1*H*, Ar–H), 7.67 (t, J = 7.5 Hz, 1*H*, Ar–H), 7.55 (s, 4*H*, Ar–H), 7.27–7.17 (m, 2*H*, Ar–H), 6.88–6.81 (m, 2*H*, Ar–H), 5.70 (s, 1*H*, N–CH), 5.50–5.29 (m, 3*H*, N–CH, O–CH_2). ^{13}C NMR (125 MHz, DMSO-d_6) δ_C: 175.4, 168.1, 167.6, 157.5, 157.0, 142.1, 135.3, 132.2, 132.0, 131.9, 129.8, 127.6, 126.9, 126.8, 126.7, 121.9, 120.5, 119.9, 116.9, 116.7, 114.9, 113.2, 62.9, 51.2. Anal. Calcd for $C_{26}H_{21}N_7O_4$ (M. wt: 495.49): C, 63.02; H, 4.27; N, 19.79; found: C, 62.96; H, 4.41; N, 20.05.

*4.1.5.2 2-(4-((2-(3-Benzyl-1,2,4-oxadiazol-5-yl)phenoxy) methyl)-1H-1,2,3-triazol-1-yl)-N′-(2-hydroxybenzylidene)acetohydrazide (**9b**).* Recrystallized from ethanol to form white solid (73% yield); m.p = 178–180 °C; R_f = 0.53 (ethyl acetate: *n*-hexane, 3 : 1); IR (KBr) ν_{max}/(cm^{-1}): 3560 (OH), 3493 (NH), 1682 (OCN), 1599 (C=N). ^{1}H NMR (500 MHz, DMSO-d_6) δ_H: 11.76 (s, 1*H*, NH), 10.10 (s, 1*H*, OH), 8.43–8.14 (m, 2*H*, Triazole–H, N=CH), 7.92 (d, J = 7.0 Hz, 1*H*, Ar–H), 7.74 (d, J = 7.5 Hz, 1*H*, Ar–H), 7.62 (t, J = 7.5 Hz, 1*H*, Ar–H), 7.55–7.49 (m, 1*H*, Ar–H), 7.30–7.21 (m, 6*H*, Ar–H), 7.11 (t, J = 10.0 Hz, 1*H*, Ar–H), 6.88–6.81 (m, 2*H*,

Ar–H), 5.67 (s, 1*H*, O–CH), 5.48–5.27 (m, 3*H*, O–CH, N–CH_2), 4.11 (s, 2*H*, Ph–CH_2). ^{13}C NMR (125 MHz, DMSO-d_6) δ_C: 175.1, 169.7, 167.6, 157.8, 157.3, 156.9, 142.3, 136.4, 135.2, 132.0, 131.8, 129.4, 129.1, 127.4, 121.8, 120.5, 120.0, 116.9, 116.7, 113.2, 62.7, 62.6, 51.3, 51.1, 31.9. Anal. Calcd for $C_{27}H_{23}N_7O_4$ (M. wt: 509.52): C, 63.65; H, 4.55; N, 19.24; found: C, 63.89; H, 4.67; N, 19.48.

*4.1.5.3 Sodium-(6-hydroxy-5-methyl-4-((2-(2-(4-((2-(3-phenyl-1,2,4-oxadiazol-5-yl)phenoxy)methyl)-1H-1,2,3-triazol-1-yl)acetyl) hydrazonol)methyl)pyridin-3-yl)methyl hydrogen phosphate (**10a**).* To give compound **10a** as brown solid (87% yield), m.p = 218–220 °C; R_f = 0.53 (EtOAc: *n*-hexane, 1 : 2); IR (KBr) ν_{max}/(cm^{-1}): 3410 (OH), 1705 (OCN). ^{1}H NMR (500 MHz, DMSO-d_6)δ_H: 14.35 (bs, 1*H*, Pyridine–OH), 12.15 (bs, 1*H*, CO–NH), 8.91 (s, 1*H*, N=C–H), 8.35 (s, 1*H*, Triazole–H), 8.08–7.84 (m, 4*H*, Ar–H), 7.67 (t, J = 7.0 Hz, 1*H*, Ar–H), 7.53 (s, 4*H*, Ar–H), 7.17 (t, J = 7.5 Hz, 1*H*, Ar–H), 5.48 (s, 2*H*, N–CH_2), 5.39 (s, 2*H*, PO–CH_2), 4.83 (s, 2*H*, O–CH_2), 2.46 (s, 3*H*, Pyridine–CH_3). ^{13}C NMR (125 MHz, DMSO-d_6) δ_C: 175.3, 168.1, 167.2, 163.7, 163.6, 157.5, 157.4, 148.8, 148.6, 147.4, 142.8, 135.3, 132.0, 131.8, 129.8, 127.6, 126.8, 121.8, 121.0, 114.9, 113.2, 62.8, 62.2, 51.3, 19.4. Anal. Calcd for $C_{27}H_{24}N_8NaO_8P$ (M. wt: 642.49): C, 50.47; H, 3.77; N, 17.44; found: C, 50.54; H, 3.96; N, 17.72.

*4.1.5.4 Sodium-(4-((2-(2-(4-((2-(3-benzyl-1,2,4-oxadiazol-5-yl) phenoxy)methyl)-1H-1,2,3-triazol-1-yl)acetyl)hydrazineylidene) methyl)-6-hydroxy-5-methylpyridin-3-yl)methyl hydrogen phosphate (**10b**).* To give compound **10b** as brown solid (61% yield), m.p = 210–212 °C; R_f = 0.53 (EtOAc: *n*-hexane, 1 : 2); IR (KBr) ν_{max}/(cm^{-1}): 3411 (OH), 1707 (OCN); ^{1}H NMR (500 MHz, DMSO-d_6) δ_H: 14.35 (bs, 1*H*, Pyridine–OH), 12.16 (bs, 1*H*, CO–NH), 8.91 (s, 1*H*, N=C–H), 8.28 (s, 1*H*, Triazole–H), 7.91 (d, J = 7.5 Hz, 2*H*, Ar–H), 7.61 (t, J = 7.0 Hz, 1*H*, Ar–H), 7.48 (d, J = 8.5 Hz, 1*H*, Ar–H), 7.29–7.19 (m, 5*H*, Ar–H), 7.10 (t, J = 8.0 Hz, 1*H*, Ar–H), 5.47 (s, 2*H*, N–CH_2), 5.34 (s, 2*H*, OP–CH_2), 4.83 (s, 2*H*, O–CH_2), 4.11 (s, 1*H*, OP–OH), 2.46 (s, 3*H*, pyridine–CH_3), 2.35 (s, 2*H*, Ph–CH_2). ^{13}C NMR (125 MHz, DMSO-d_6) δ_C: 175.0, 172.9, 169.7, 163.6, 157.3, 148.9, 147.4, 142.8, 141.4, 139.7, 139.3, 136.4, 135.1, 131.7, 129.5, 129.1, 127.3, 126.8, 121.7, 121.0, 115.1, 114.9, 113.3, 62.8, 51.3, 31.9. Anal. Calcd for $C_{28}H_{26}N_8NaO_8P$ (M. wt: 656.52): C, 51.23; H, 3.99; N, 17.07; found: C, 51.52; H, 4.15; N, 17.34.

4.1.6. General methedolgy for carbothioamide 11a and 11b. Phenyl isothiocyanate (50 mg, 0.37 mmol) was added to a solution of Compound **8a** or **8b** (0.13 mmol) in absolute ethanol (20 mL) and the mixture was refluxed for 8 h. The reaction was monitored by TLC. After completion, the reaction mixture was kept to cool at room temperature. The formed precipitated solid was collected by filtration, dried and crystallized from ethanol to give.

*4.1.6.1 N-Phenyl-2-(2-(4-((2-(3-phenyl-1,2,4-oxadiazol-5-yl) phenoxy)methyl)-1H-1,2,3-triazol-1-yl)acetyl)hydrazine-1-carbothioamide (**11a**).* **11a** white solid (80% yield); m.p = 115–117 °C; R_f = 0.53 (EtOAc: *n*-hexane, 1 : 2); IR (KBr) ν_{max}/(cm^{-1}): 3216 (NH), 1688 (OCN), 744 (C=S); ^{1}H NMR (500 MHz, DMSO-d_6) δ_H: 11.04 (s, 1*H*, N–H), 9.80 (s, 1*H*, NH), 8.30 (s, 1*H*, Triazole–H), 8.08–8.03 (m, 2*H*, Ar–H), 7.69–7.53 (m, 4*H*, CO–NH, Ar–H), 7.37–7.30 (m, 6*H*, Ar–H), 7.19–7.10 (m, 3*H*, Ar–H), 5.40, 5.24 (2s, 2*H*, N–CH_2), 4.84 (s, 2*H*, O–CH_2).^{13}C NMR (125 MHz, DMSO-d_6) δ_C: 175.5, 168.2, 168.1, 157.5, 142.8, 139.1, 139.0, 135.3, 132.1, 131.9, 129.9, 129.4, 129.0, 128.7, 127.6, 126.8, 122.2, 121.9, 114.9, 113.2, 67.8, 65.7, 62.7, 51.1. Anal. Calcd for $C_{26}H_{22}N_8O_3S$ (M. wt: 526.57): C, 59.31; H, 4.21; N, 21.28; found: C, 59.52; H, 4.13; N, 21.43.

*4.1.6.2 2-(2-(4-((2-(3-Benzyl-1,2,4-oxadiazol-5-yl)phenoxy) methyl)-1H-1,2,3-triazol-1-yl)acetyl)-N-phenylhydrazine-1-carbothioamide (**11b**).* **11b** (76% yield); m.p = 95–97 °C; R_f = 0.53 (EtOAc: *n*-hexane, 1 : 2); IR (KBr) ν_{max}/(cm^{-1}): 3216 (NH), 1596 (OCN), 741 (C=S). ^{1}H NMR (500 MHz, DMSO-d_6) δ_H: 11.0 (s, 3*H*, 3NH), 7.60 (bs, 2*H*, Triazole–H, Ar–H), 7.30 (s, 10*H*, Ar–H), 7.09 (bs, 3*H*, Ar–H), 4.48 (s, 6*H*, Ph–CH_2, N–CH_2, O–CH_2). ^{13}C NMR (125 MHz, DMSO-d_6) δ_C: 188.4, 187.7, 139.2, 139.1, 139.0, 138.9, 138.6, 138.4, 138.3, 129.4, 129.0, 125.6, 125.1, 123.6, 122.2, 67.8, 65.7, 14.5. Anal. Calcd for $C_{27}H_{24}N_8O_3S$ (M. wt: 540.60): C, 59.99; H, 4.47; N, 20.73; S, 5.93; found: C, 60.12; H, 4.45; N, 20.44.

4.2. Biological activity

4.2.1. Cytotoxic evaluation (IC_{50}) on A549 and Caco-2 cell lines. The anticancer evaluation was performed *via* MTT assay[40] and the procedure is detailed in the ESI data.†

4.2.2. Cytotoxicity screening on normal lung fibroblast WI38. Cytotoxicity evaluation was tested *via* MTT assay[40] as mentioned in the ESI data.†

4.2.3. Mechanistic study: PI3K/mTOR/EGFR/P53 in A549 and Caco-2. 5*104 cells were plated in each well of a 12-well plate, and the plate was then incubated in a CO2-rich incubator (37 °C, 5% CO_2, and 90% relative humidity) for a whole day. Following the incubation time, 750 μL of the IC50 of each chemical was added, and the plate was incubated for 24 hours in a CO_2 incubator (37 °C, 5% CO_2, and 90% relative humidity). The plate was then centrifuged at 1650 rpm for 5 minutes, and the supernatants were disposed of. The plate was centrifuged after the incubation period, and the cell plate was then exposed to RNA isolation using an RNA isolation kit (iNtRON Biotechnology, Korea) in accordance with the manufacturer's instructions. Using the sensiFAST cDNA synthesis kit (Bioline, London), RNA was transformed into cDNA. B-actin was used as a housekeeping gene in the qPCR gene amplification process. 12.5 μL of SensiFAST SYBR (Bioline, London) was combined with 1 μL of cDNA, 0.5 μL of forward primer (10 pmol mL^{-1}) and 0.5 μL of reverse primer (10 pmol mL^{-1}) for every primer (Table 6). The volume was then brought to 20 μL using distilled water devoid of nuclease. Using a CFX96TM Real-Time System (BIO-RAD, USA), samples were put in the cycler and the programme started with one cycle of 95 °C for 10 min (initial denaturation), followed by 40 cycles of 95 °C for 15 s (denaturation), 60 °C for 30 s (annealing), and 72 °C for 30 s (extension). To determine the fold change in target genes, the $2 - \Delta\Delta C_t$ method was used to normalise the quantities critical threshold (C_t) of the target gene with quantities (C_t) of the house-keeping gene.

4.2.4. Docking study. Molecular operating environment (MOE 2014.09) software was used to conduct all of the docking investigations in this work.[41,42] From the protein databank, with

the ID 2ITY, we obtained the X-ray crystal structures of EGFR complexed with gefitinib. First, the receptors' hydrogens and charges were adjusted with the help of AMBER10: EHT integrated into MOE. The binding site was determined according to site where the co-crystallized ligand is bound. Following this, the EGFR binding domain was docked with compounds **6a**, **6b**, **8a** and **11b** using triangular matcher and London dg, respectively, as placement and scoring methods. Finally, the discovery studio visualizer was used to produce 2D and 3D interaction diagrams to analyse the docking outcomes.

Conflicts of interest

The authors declare that none of their relationships or conflicting financial interests could have influenced the findings of this study.

Acknowledgements

"MSA acknowledge the Deanship of Scientific Research, Vice Presidency for Graduate Studies and Scientific Research, King Faisal University, Saudi Arabia for financial support under the annual funding track [Project No. GrantA316]".

References

1 S. Jin, Y. Sun, X. Liang, X. Gu, J. Ning, Y. Xu, S. Chen and L. Pan, Emerging new therapeutic antibody derivatives for cancer treatment, *Signal Transduction Targeted Ther.*, 2022, **7**, 39.
2 S. Sigismund, D. Avanzato and L. Lanzetti, Emerging functions of the EGFR in cancer, *Mol. Oncol.*, 2018, **12**, 3–20.
3 J.-P. Spano, C. Lagorce, D. Atlan, G. Milano, J. Domont, R. Benamouzig, A. Attar, J. Benichou, A. Martin and J.-F. Morere, Impact of EGFR expression on colorectal cancer patient prognosis and survival, *Ann. Oncol.*, 2005, **16**, 102–108.
4 W. Pao and J. Chmielecki, Rational, biologically based treatment of EGFR-mutant non-small-cell lung cancer, *Nat. Rev. Cancer*, 2010, **10**, 760–774.
5 S. J. Rogers, K. J. Harrington, P. Rhys-Evans, P. O-Charoenrat and S. A. Eccles, Biological significance of c-erb B family oncogenes in head and neck cancer, *Cancer Metastasis Rev.*, 2005, **24**, 47–69.
6 J. C. Lee, I. Vivanco, R. Beroukhim, J. H. Y. Huang, W. L. Feng, R. M. DeBiasi, K. Yoshimoto, J. C. King, P. Nghiemphu and Y. Yuza, Epidermal growth factor receptor activation in glioblastoma through novel missense mutations in the extracellular domain, *PLoS Med.*, 2006, **3**, e485.
7 M. Oliveira-Cunha, W. G. Newman and A. K. Siriwardena, Epidermal growth factor receptor in pancreatic cancer, *Cancers*, 2011, **3**, 1513–1526.
8 H.-W. Lo, S.-C. Hsu and M.-C. Hung, EGFR signaling pathway in breast cancers: from traditional signal transduction to direct nuclear translocalization, *Breast Cancer Res. Treat.*, 2006, **95**, 211–218.
9 S. Yan, H. Wu, Y. Zhu, S. Shen, K. Zhang, W. Wu and N. Liu, FGFC1 selectively inhibits erlotinib-resistant non-small cell lung cancer *via* elevation of ROS mediated by the EGFR/PI3K/Akt/mTOR pathway, *Front. Pharmacol*, 2022, **12**, 764699.
10 R. B. Cohen, Epidermal growth factor receptor as a therapeutic target in colorectal cancer, *Clin. Colorectal Cancer*, 2003, **2**, 246–251.
11 B. Pabla, M. Bissonnette and V. J. Konda, Colon cancer and the epidermal growth factor receptor: Current treatment paradigms, the importance of diet, and the role of chemoprevention, *World J. Clin. Oncol.*, 2015, **6**, 133.
12 Y. He, M. M. Sun, G. G. Zhang, J. Yang, K. S. Chen, W. W. Xu and B. Li, Targeting PI3K/Akt signal transduction for cancer therapy, *Signal Transduct. Targeted Ther.*, 2021, **6**, 425.
13 R. Liu, Y. Chen, G. Liu, C. Li, Y. Song, Z. Cao, W. Li, J. Hu, C. Lu and Y. Liu, PI3K/AKT pathway as a key link modulates the multidrug resistance of cancers, *Cell Death Dis.*, 2020, **11**, 797.
14 Y. Peng, Y. Wang, C. Zhou, W. Mei and C. Zeng, PI3K/Akt/mTOR pathway and its role in cancer therapeutics: are we making headway?, *Front. Oncol.*, 2022, **12**, 819128.
15 L. Yu; J. Wei and P. Liu Attacking the PI3K/Akt/mTOR signaling pathway for targeted therapeutic treatment in human cancer, in *Proceedings of the Seminars in Cancer Biology*, 2022, pp. 69–94.
16 J. Bang, M. Jun, S. Lee, H. Moon and S. W. Ro, Targeting EGFR/PI3K/AKT/mTOR signaling in hepatocellular carcinoma, *Pharmaceutics*, 2023, **15**, 2130.
17 M. Colardo, M. Segatto and S. Di Bartolomeo, Targeting RTK-PI3K-mTOR axis in gliomas: An update, *Int. J. Mol. Sci.*, 2021, **22**, 4899.
18 A. J. Levine and A. M. Puzio-Kuter, The control of the metabolic switch in cancers by oncogenes and tumor suppressor genes, *Science*, 2010, **330**, 1340–1344.
19 M. M. Alam, 1, 2, 3-Triazole hybrids as anticancer agents: a review, *Arch. Pharm.*, 2022, **355**, 2100158.
20 G. Mohan, G. Sridhar, E. Laxminarayana and M. T. Chary, Synthesis and biological evaluation of 1, 2, 4-oxadiazole incorporated 1, 2, 3-triazole-pyrazole derivatives as anticancer agents, *Chem. Data Collect.*, 2021, **34**, 100735.
21 K. Bozorov, J. Zhao and H. A. Aisa, 1, 2, 3-Triazole-containing hybrids as leads in medicinal chemistry: A recent overview, *Bioorg. Med. Chem.*, 2019, **27**, 3511–3531.
22 M. A. Mahmoud, A. F. Mohammed, O. I. Salem, H. A. Gomaa and B. G. Youssif, New 1, 3, 4-oxadiazoles linked with the 1, 2, 3-triazole moiety as antiproliferative agents targeting the EGFR tyrosine kinase, *Arch. Pharm.*, 2022, **355**, 2200009.
23 S. K. Verma, R. Verma, K. S. S. Kumar, L. Banjare, A. B. Shaik, R. R. Bhandare, K. P. Rakesh and K. S. Rangappa, A key review on oxadiazole analogs as potential methicillin-resistant Staphylococcus aureus (MRSA) activity: Structure-activity relationship studies, *Eur. J. Med. Chem.*, 2021, **219**, 113442.
24 S. K. Verma, R. Verma, Y. R. Girish, S. Verma, K. Pramoda, Y. Vaishnav, J. Saji and K. S. S. Kumar, Two-dimensional Ti_3C_2Tx MXenes as a catalyst support for the synthesis of

1, 4-disubstituted-1, 2, 3-triazoles *via* azide-nitroalkene oxidative cycloaddition, *J. Mol. Struct.*, 2023, **1281**, 135145.
25 Y. Hu, Z. Liu, G. Zha, S. Long, M. Sridhara, K. S. S. Kumar and K. P. Rakesh, Triazole derivatives as potential antifungal agents: A structure-activity relationship (SAR) studies, *Process Biochem.*, 2023, 102–118.
26 S. Mandal, S. Mandal, S. Biswas, S. Banerjee and B. Saha, Synthesis of 2-(ethynyloxy) naphthaene-1-carbaldehyde using 2-hydroxy benzyl alcohol and propargyl bromide in aqueous micellar media, *Res. Chem. Intermed.*, 2018, **44**, 2169–2177.
27 M. S. Singh, S. Chowdhury and S. Koley, Advances of azide-alkyne cycloaddition-click chemistry over the recent decade, *Tetrahedron*, 2016, **72**, 5257–5283.
28 A. Amadasi, M. Bertoldi, R. Contestabile, S. Bettati, B. Cellini, M. Luigi di Salvo, C. Borri-Voltattorni, F. Bossa and A. Mozzarelli, Pyridoxal 5'-phosphate enzymes as targets for therapeutic agents, *Curr. Med. Chem.*, 2007, **14**, 1291–1324.
29 A. Bolje, D. Urankar and J. Košmrlj, Synthesis and NMR Analysis of 1, 4-Disubstituted 1, 2, 3-Triazoles Tethered to Pyridine, Pyrimidine, and Pyrazine Rings, *Eur. J. Org Chem.*, 2014, **2014**, 8167–8181.
30 F. M. Freimoser, C. A. Jakob, M. Aebi and U. Tuor, The MTT [3-(4, 5-dimethylthiazol-2-yl)-2, 5-diphenyltetrazolium bromide] assay is a fast and reliable method for colorimetric determination of fungal cell densities, *Appl. Environ. Microbiol.*, 1999, **65**, 3727–3729.
31 M. El-Zeftawy, D. Ghareeb, E. R. ElBealy, R. Saad, S. Mahmoud, N. Elguindy, A. F. El-kott and M. El-Sayed, Berberine chloride ameliorated PI3K/Akt-p/SIRT-1/PTEN signaling pathway in insulin resistance syndrome induced in rats, *J. Food Biochem.*, 2019, **43**, e13049.
32 D. A. Guertin and D. M. Sabatini, Defining the role of mTOR in cancer, *Cancer Cell*, 2007, **12**, 9–22.
33 G. Lurje and H.-J. Lenz, EGFR signaling and drug discovery, *Oncology*, 2010, **77**, 400–410.
34 J. T. Zilfou and S. W. Lowe, Tumor suppressive functions of p53, *Cold Spring Harbor Perspect. Biol.*, 2009, **1**, a001883.
35 A. Daina, O. Michielin and V. Zoete, SwissADME: a free web tool to evaluate pharmacokinetics, drug-likeness and medicinal chemistry friendliness of small molecules, *Sci. Rep.*, 2017, **7**, 42717.
36 C. A. Lipinski, F. Lombardo, B. W. Dominy and P. J. Feeney, Experimental and computational approaches to estimate solubility and permeability in drug discovery and development settings, *Adv. Drug Delivery Rev.*, 1997, **23**, 3–25.
37 D. F. Veber, S. R. Johnson, H.-Y. Cheng, B. R. Smith, K. W. Ward and K. D. Kopple, Molecular properties that influence the oral bioavailability of drug candidates, *J. Med. Chem.*, 2002, **45**, 2615–2623.
38 M. Maximo da Silva, M. Comin, T. Santos Duarte, M. A. Foglio, J. E. De Carvalho, M. do Carmo Vieira and F. A. S. Nazari, Synthesis, antiproliferative activity and molecular properties predictions of galloyl derivatives, *Molecules*, 2015, **20**, 5360–5373.
39 E. Ostertagová and O. Ostertag, Methodology and Application of One-way ANOVA, *Am. J. Mech. Eng.*, 2013, **1**, 256–261.
40 T. Mosmann, Rapid colorimetric assay for cellular growth and survival: application to proliferation and cytotoxicity assays, *J. Immunol. Methods*, 1983, **65**, 55–63.
41 C. Scholz, S. Knorr, K. Hamacher and B. Schmidt, DOCKTITE A Highly Versatile Step-by-Step Workflow for Covalent Docking and Virtual Screening in the Molecular Operating Environment, *J. Chem. Inf. Model.*, 2015, **55**, 398–406.
42 S. Vilar, G. Cozza and S. Moro, Medicinal chemistry and the molecular operating environment (MOE): application of QSAR and molecular docking to drug discovery, *Curr. Top. Med. Chem.*, 2008, **8**, 1555–1572.